Excitation of optically trapped single particles using femtosecond pulses

KYLE S. LATTY[1,*], JUSTIN BORRERO[1], THIAGO ARNAUD[1], AND KYLE C. HARTIG[1]

[1] *Nuclear Engineering Program, Department of Materials Science and Engineering, University of Florida, Gainesville, FL 32611, USA*
[*] *klatty@ufl.edu*

Compiled June 13, 2024

Excitation from optically trapped particles are examined through laser-induced breakdown spectroscopy following interactions with mJ-level fs-pulses. The optical emissions from sub-ng ablation of precisely positioned cupric oxide microparticles are used as a method to spatially resolve the laser-particle interactions resulting in excitation. External focusing lenses are often used to change the dynamics of nonlinear self-focusing of fs-pulses to form laser filaments, or alternatively, to form very intense air plasmas. Given the significant implications external focusing has on the laser propagation and plasma conditions, single-particle emissions are studied with focusing lenses ranging from 50-300 mm. It is shown that, while single particles are less excited at longer focal lengths due to limited energy transfer through laser-particle interactions, the cooler plasma results in a lower thermal background to reveal resolved single-shot emission peaks. By developing an understanding in the fundamental interaction that occurs between single-particles and fs-pulses and filaments, practical improvements can be made for atmospheric remote sensing of low-concentration aerosols.

http://dx.doi.org/10.1364/ao.XX.XXXXXX

Monitoring and characterizing aerosols using laser-induced breakdown spectroscopy (LIBS) is a growing effort that aims to achieve rapid analytical measurements from laser-produced plasma (LPP) emissions, gaining particular attraction as a tool for atmospheric sensing [1–3] and for nuclear treaty verification [4]. However, measuring atmospheric aerosols presents several challenges in LIBS owing to the complex spatiotemporal plasma-particle and laser-particle interactions required to yield emissions from particle analytes [5–7]. In a highly inhomogenous LPP, the rate of energy and mass transfer is highly dependent on the position of the particle relative to the plasma, giving rise to strong spatial dependencies in the emission signal [8, 9]. Furthermore, given the unrepeatable nature of any single plasma-particle interaction in a bulk aerosol, experimentally studying the mechanisms of the particle excitation process remains a difficult research endeavor beyond computational efforts [10].

Optical traps (OT) have become increasingly popular as a tool to facilitate precise manipulation of particles in air [11], resulting in several studies that examine spatially-resolved interaction of particles in LPPs resulting from air breakdown using ns-laser pulses [9, 12–16]. The excitation process is known to dramatically change as the pulse duration approach ultrafast limits (1 ps) in both solid and aerosol samples [17], yet analogous studies that examine particle interactions with ultrafast pulses are sparse. It has been recently shown through OT-LIBS, that using 100-ps pulses improves the signal-to-noise ratio compared to 6-ns pulses due to reduced thermal effects in the LPP, resulting in attogram detection limits [18]. At shorter fs-pulse durations, the ionization pathways in air begins to shift from multiphoton ionization to tunnel ionization, affecting the subsequent plasma characteristics [19, 20]; however, the exact consequence of this action on plasma-particle and laser-particle interactions remains unexplored. Furthermore, high-power fs-pulses will naturally undergo nonlinear self-focusing after several meters of free-air propagation to form laser filaments. In most cases, aerosols are measured by loosely-focusing the pulse to form filaments prior to the geometric focus [21] or by tightly-focusing the pulse to form very intense plasmas [22]. Given filamentation is sustained through the balance between focusing effects (e.g. external focusing and self-focusing) and defocusing effects (e.g. diffraction and plasma defocusing), understanding the effects of external focusing on the laser-propagation behavior and subsequent particle interaction is critical to improve standoff aerosol sensing.

In this Letter, we demonstrate the use of focused fs-pulses to excite and perform spatiotemporally-resolved LIBS on single, micron-sized cupric oxide particles in an OT. Using focusing lenses ranging from 50-300 mm (f/1.97-11.8), it is shown that both the single-particle emissions and the thermal background are drastically reduced at longer focal lengths, corresponding to a shift towards lower energy levels in the excited state population of Cu. At the longest focal length, a thin plasma column is formed from photoionzation that is estimated to be less than 100 µm in diameter; thus, the OT system is designed to manipulate the particle position along the transverse plane of the beam profile to be in the most intense region of the laser field to result in laser-particle interactions.

The experimental setup used for OT-LIBS is shown in Fig. 1 with a reference coordinate system. A chirped pulse amplified Ti:Sapphire laser (Coherent Astrella) is used to generate 35 fs pulses at a center wavelength of 800 nm. The pulse energy is measured to be 5.3 mJ, resulting in a peak power of

0.15 TW which exceeds the critical power for self-focusing in air (P_{cr}) by a factor of 15 [23]. Given that the peak power exceeds the critical power by an order of magnitude, even under shorter focusing conditions, multiple filaments are expected to form that rapidly bunch together towards the geometric focus to form an intense plasma [24]. The focal length of the focusing lenses used in this experiment are $f = 50, 100, 150, 200, 300$ mm (f/n $= 1.96, 3.92, 5.90, 7.87, 11.8$), and the beam path is propagated along the y-axis. An optical chopper is used to reduce the repetition rate of the pulse train from 1 kHz down to 125 Hz such that an optical shutter with an opening time of 6 ms can be used to control the passage of the fs-pulses and trigger measurements after particles have been trapped. Particle emissions are collected using a 5×microscope objective along the x-axis and the emission light is focused onto an optical fiber attached to a Czerny-Turner spectrometer (Princeton Instruments HRS-500) with an emICCD detector (Princeton Instruments PI-MAX4). Using a 1200 gr/mm grating, the instrumental broadening was measured to be 0.237 nm at full-width half-maximum (FWHM) using a mercury lamp source.

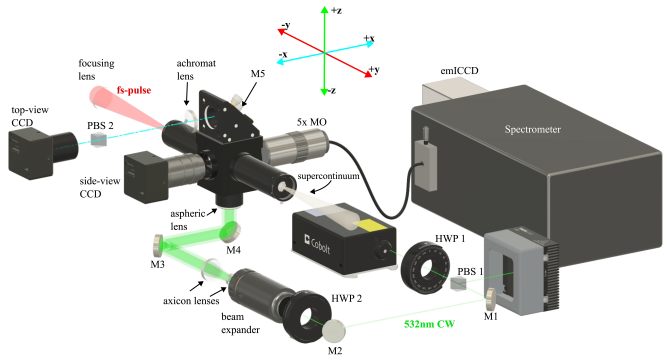

Fig. 1. Experimental setup for optical trapping and fs-LIBS. Components are abbreviated as mirrors (M), half-wave plates (HWP), and polarizing beamsplitter (PBS).

For the OT component of the experiment, a continuous wave 532 nm laser (Cobolt Samba) with a maximum power of 1 W and an initial beam diameter of 800 µm is used. After expanding the beam to ∼10 mm, dual axicon lenses with apex angles of 10 °are used to form a collimated hollow beam. Hollow beams have been demonstrated to improve the trapping efficiency compared to single Gaussian beams and exhibits potential as a universal optical trap, capable of trapping absorptive and transparent particles through photophoretic and radiative pressure forces, respectively [11, 25]. Prior to the vertical mirror (M4), the hollow beam is directed perpendicular to the beam path of fs-pulse along the +x axis. The $NA = 0.66$ aspheric lens and mirror (M4) are assembled on an x-axis translation stage, and given the beam path is parallel to the vector of translation, alignment is retained as particles are manipulated along the x-axis. The height of the particle along the z-axis is adjusted by mounting the aspheric lens on a separate z-axis translation stage, allowing precise positioning of the particle along the x-z plane while retaining optimal alignment. The particle is trapped in a custom 3D printed chamber (40×40×33 mm) with an elevated bottom platform to trap particles near the center of the chamber using the short working distance aspheric lens (11.27 mm). The chamber includes small openings to avoid damage from the filaments and to reduce scattering from the laser light and generated supercontinuum.

By adjusting the power of the OT laser to ∼400 mW using a half-wave plate (HWP1) and polarizing beam splitter cube (PBS1), cupric oxide particles ranging from 1-5 µm are readily trapped in air for several hours without significant positional deviations relative to the size of the filament (100 µm). Multiple particles can be photophoretically trapped at 400 mW in some of the dark regions of the beam profile, in which case the power is slowly reduced until a single particle remains in the trap. The scattered light from the trapped particle is monitored in the z-axis using a side-view CCD camera (Mightex) as shown in Fig. 2(a), and also serves to align the 5×microscope objective for optimal light collection. The top-view CCD camera in Fig. 2(b) monitors the particle position along the x-axis after filtering the hollow beam light using a half-wave plate (HWP 2) before the trap and a polarizing beamsplitter cube (PBS 2) after the trap.

Aligning the fs-pulses to the trapping region begins by first trapping a particle after inserting them with a pipette, and aligning the light collection optics by maximizing the spectroscopic signal from the scattered 532 nm light. Next, while passing the fs-pulses through the chamber, the position of the focusing lens is adjusted along the y-axis until the spectroscopic signal from the N_2^+ first negative system ($B^2\Sigma_u^+ \rightarrow X^2\Sigma_g^+$) (0,0) band originating from the filament excitation is maximized using a 3-ns gate delay and a 5-ns exposure time, such that the particles are positioned in the most photoionized region in the laser field [26]. To measure the N_2^+ signal, the collection optic is translated along the z-axis to match the height of the fs-beam path. The filament is imaged using a 391±1.5 nm bandpass filter to isolate the N_2^+ fluorescence on both CCDs as shown in Fig. 2, and the position is marked. At this point, particles can be trapped and manipulated along the x-z plane to the marked position of the fs-pulse beam path to complete the alignment procedure. For each focusing lens, 10 separate cupric oxide particles are isolated in the trap and the time-resolved Cu I emissions are measured using a 20-ns gate delay and a 1-µs exposure time. Integrated emission intensities are measured by fitting a Voigt profile and a linear background to the Cu I peaks and extracting the amplitude from each single-shot spectrum.

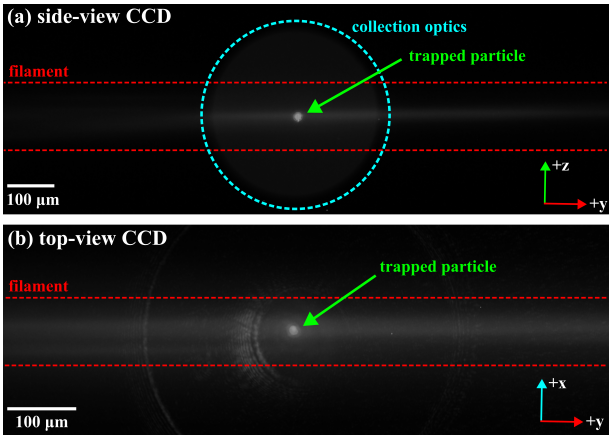

Fig. 2. (a) Side-view CCD with overlapped images of a trapped particle, the fs-plasma, and backpropagated light through the light collection optics. (b) Top-view CCD with overlapped images of a trapped particle and the fs-plasma. The images demonstrate alignment using a 100 mm focusing lens.

The 10-shot averaged spectrum for each focusing lens laser

ablation condition is shown in Fig. 3(a), and the extracted amplitude from the Cu I 510.55 nm peak from each individual laser shot is plotted in sequential order in Fig. 3(b). Aside from Cu, emissions from Mg were found in some of the single-shot spectra, and thus it can be assumed that Mg is inhomogenously mixed in the cupric oxide matrix as a minor contaminant. The particle size distribution ranges from 1-5 µm, corresponding to a factor of 125 difference in mass and volume between the upper and lower limit of the distribution. If particles are dissociated to near completion, a linear relationship between the particle mass and the measured emission signal is to be expected [13, 27]. The fluctuation between the maximum and minimum signal intensity never exceeded a factor 20, indicating size-selectivity in the OT or possibly incomplete dissociation of larger particles, forming an upper limit to particle excitation. Size-selectivity, in this case of photophoretic trapping, is improved by only measuring particles that are trapped in the same region of the OT [12]. Within any region of the OT with a constant irradiance profile, only a limited range of particle sizes can meet the balance between gravitational force and photophoretic force to result in a stable trap. For this experiment, only particles trapped in the center of the OT beam profile as shown in Fig. 2(b) were measured. Smaller particles that were occasionally trapped in the walls of the hollow beam were removed by lowering the OT power.

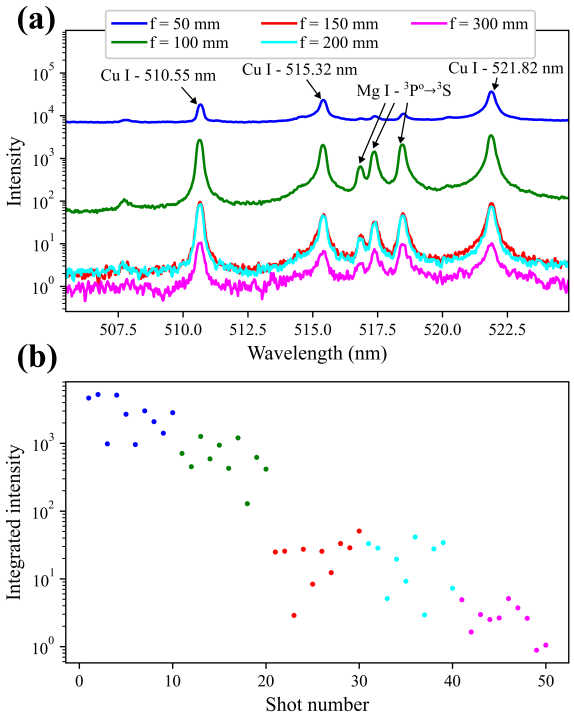

Fig. 3. (a) Averaged spectrum of Cu for each focusing lens condition used for 10 individually trapped cupric oxide particles. (b) The integrated intensity from each single-shot spectrum is extracted from Cu I 510.55 nm and are plotted in the sequence.

It is apparent that the emission intensity from Cu rapidly decreases using longer focusing lenses from Fig. 3(b). It is also noticeable that the ratio of the Cu emission peaks are dependent on the focusing condition. The integrated intensities (I) of Cu I 510.55 nm and Cu I 515.32 nm are compared in Table 1. Most measurements show a relative standard deviation close to 50% of the mean, which is largely attributed to the polydisperse particle size distribution. The intensity ratio between Cu I 510.55 nm and Cu I 515.32 nm ($I_{510.55\ \mathrm{nm}} / I_{515.55\ \mathrm{nm}}$) consistently increases with focal length. The upper energy levels for the 510.55 nm and the 515.32 nm transitions are 3.82 eV and 6.19 eV, respectively. Thus, the ratio $I_{510.55\ \mathrm{nm}} / I_{515.55\ \mathrm{nm}}$ reflects a downward shift in the population of the excited states of Cu, indicating a reduction in energy transfer to the particle. This is also evidence by the reduction in the thermal background seen in Fig. 3(a).

Table 1. Integrated intensities of Cu

f (mm)	$I_{510.55\ \mathrm{nm}}$	$I_{515.55\ \mathrm{nm}}$	$I_{510.55\ \mathrm{nm}} / I_{515.55\ \mathrm{nm}}$
50	2910±1550	5680±2928	0.523
100	677±345	510±266	1.14
150	24.0±12.9	15.7±9.15	1.39
200	20.9±13.2	11.1±7.76	1.68
300	2.81±1.38	1.74±0.909	2.00

A broader background measurement is taken and shown in Fig. 4(a), where the instrumental response function is corrected using a calibrated tungsten lamp. Here, the fluorescence from N_2^+ used during alignment is shown, along with the H-α peak at 656.28 nm. The electron density is determined from the FWHM of the H-α peak, where the Stark broadening is extracted assuming a reduced Stark profile FWHM of $\alpha_{1/2} = 1.34 \times 10^{-3}$ nm and a 0.237 nm contribution to the FWHM due to instrumental broadening. The H-α signal is too weak for the 300 mm focusing lens condition, so the electron density cannot be determined.

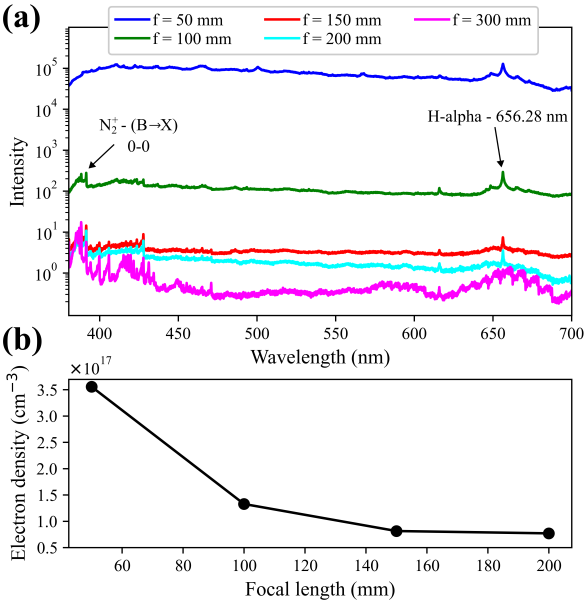

Fig. 4. (a) Broadband background spectrum for each focusing lens condition without trapped particles. (b) The electron density is estimated from the Stark broadening of the H-α line, excluding the 300 mm focusing lens condition.

The electron density decreases by approximately an order of magnitude from the 50 mm focusing lens to the 200 mm focusing lens, similar to the trends reported by Théberge *et al.* [28]. In a

previous study, the electron density was also shown to decrease with longer focusing conditions when the electron density was extracted from the emissions of bulk Sr aerosols using a 400 mm and 750 mm focusing lens; however, the maximum electron density was shown to only change by a factor of 1.5 [29]. Based on the extracted electron densities and the rapid decrease of the thermal background from using the 50 mm to 100 mm focusing lens in Fig. 4(a), acute changes in the plasma characteristics are supported to occur for shorter focusing conditions, requiring higher electron densities to counteract the strong focusing effects through plasma defocusing [28].

At this point, it is important to form a distinction between laser-particle and plasma-particle interactions. Unlike plasma-particle interactions, which are characterized by emission resulting from electron impact ionization, laser-particle interactions are driven by direct photoionization. While both the Cu emission and electron density is shown to decrease at longer focal lengths, this does not necessary mean the Cu emission is a result of plasma-particle interactions, as the electron density of the plasma for fs-pulses is closely related to the focused laser intensity [30]. In ns-LIBS, most particle emission are commonly assumed to be a result of plasma-particle interactions due to the larger expansion of the ns-LPP from air breakdown, expanding to dimensions upwards of 1.5 mm in diameter that far exceed the typical dimension of the spot size at the breakdown threshold in air [7, 8]. This assumption does not hold for this experiment, as particles are positioned where the the short-lived N_2^+ fluorescence is the most intense during the alignment procedure with 5 µm precision. The ionization threshold of N_2 is 15.6 eV, and the measured N_2^+ fluorescence used during alignment results from direct photoionization in the form of multiphoton ionization or tunnel ionization in the most intense region of the laser field [26]. Thus, positioning particles largely comprised of Cu with a lower ionization threshold of 7.72 eV directly where the short-lived N_2^+ fluorescence exists would result in laser-particle interactions. In this case, particle excitation is caused directly by the laser fluence interactive at the particle surface. As intensity-clamped limits are approached under longer focusing conditions through laser filamentation [31], particle excitation is naturally expected to experience a similar limitation through laser-particle energy coupling which explains the reduced emission intensities at longer focal lengths in Fig. 3(b). This is unlike filament interactions with bulk solid samples, where the entire pulse energy is deposited directly onto the sample surface resulting in stronger Cu emissions [32]. Here, only a small portion of the filament is expected to interact and transfer energy to the particle given the relative size difference between the filaments ($\sim$100 µm) and the particle ($<$5 µm).

In summary, a vertical hollow beam OT was used to precisely manipulate particles along a 2D plane to intersect with the beam path of a focused fs-pulse. The emission spectrum was measured through LIBS, and the particle emissions from Cu in cupric oxide microparticles were shown to rapidly decrease as the focal length was increased from 50 mm to 300 mm. A similar decrease is seen with the thermal background, and by extracting the Stark broadening contribution to the FWHM of the H-α line, the free electron density is estimated to also decrease by an order of magnitude as the focal length is increased from 50 mm to 200 mm. The intensity ratio between Cu I 510.55 nm and Cu I 515.32 nm is also increased for longer focusing conditions, suggesting a shift towards lower energy levels in the distribution of the excited state population. Together, particle excitation is evidenced to progressively weaken towards longer focusing conditions that approach the regime of filamentation, where particle ionization is limited by the laser-particle energy transfer in intensity-clamped pulses. Intensity clamping limits the fluence at the particle surface, thus, for any given particle of equivalent size and composition, it is expected that energy transfer is inherently limited when interacting with a laser filament.

Funding. Defense Threat Reduction Agency (HDTRA1-20-2-0002) and National Nuclear Security Administration (DE-NA0004142).

Acknowledgments. The authors acknowledge the support provided by the Department of Defense Science, Mathematics, and Research for Transformation (SMART) Scholarship-for-Service Program.

Disclosures. The authors declare no conflicts of interest.

Data availability. Data underlying the results presented in this paper are not publicly available at this time but may be obtained from the authors upon reasonable request.

REFERENCES

1. Y. Zhang, T. Zhang, and H. Li, Spectrochimica Acta Part B: At. Spectrosc. **181**, 106218 (2021).
2. H. Ji, Y. Ding, L. Zhang, *et al.*, Appl. Spectrosc. Rev. **56**, 193 (2021).
3. D. W. Hahn and M. M. Lunden, Aerosol Sci. Technol. **33**, 30 (2000).
4. E. H. Kwapis, J. Borrero, K. S. Latty, *et al.*, Appl. Spectrosc. **78**, 9 (2024).
5. M. Z. Martin, M.-D. Cheng, and R. C. Martin, Aerosol Sci. Technol. **31**, 409 (1999).
6. P. Diwakar, P. Jackson, and D. Hahn, Spectrochimica Acta Part B: At. Spectrosc. **62**, 1466 (2007).
7. K. S. Latty and K. C. Hartig, Appl. Spectrosc. p. 000370282211494 (2022).
8. V. Hohreiter and D. W. Hahn, Anal. Chem. **78**, 1509 (2006).
9. P. Purohit, F. J. Fortes, and J. J. Laserna, Spectrochimica Acta Part B: At. Spectrosc. **130**, 75 (2017).
10. P. Dalyander, I. Gornushkin, and D. Hahn, Spectrochimica Acta Part B: At. Spectrosc. **63**, 293 (2008).
11. Z. Gong, Y.-L. Pan, G. Videen, and C. Wang, J. Quant. Spectrosc. Radiat. Transf. **214**, 94 (2018).
12. T. Liu, X. Cheng, Q. Zhang, *et al.*, Talanta **268**, 125326 (2024).
13. F. J. Fortes, P. Purohit, and J. J. Laserna, Spectrochimica Acta Part B: At. Spectrosc. **180**, 106193 (2021).
14. C. Niu, Z. Hu, X. Cheng, *et al.*, Anal. Chem. **95**, 2874 (2023).
15. S. T. Järvinen, S. Saari, J. Keskinen, and J. Toivonen, Spectrochimica Acta Part B: At. Spectrosc. **99**, 9 (2014).
16. P. Purohit, F. J. Fortes, and J. Laserna, Nano Res. **16**, 7470 (2023).
17. E. Gamaly and A. Rode, Prog. Quantum Electron. **37**, 215 (2013).
18. C. Burgos-Palop, P. Purohit, F. J. Fortes, and J. Laserna, Anal. Chem. **95**, 14541 (2023).
19. S. L. Chin and H. Xu, J. Phys. B: At. Mol. Opt. Phys. **49**, 222003 (2016).
20. V. Tamulienė, G. Juškevičiūtė, D. Buožius, *et al.*, Sci. Reports **10**, 17437 (2020).
21. Z. Zhang, N. Zhang, Y. Wang, *et al.*, Opt. Express **31**, 6464 (2023).
22. P. A. Babushkin, G. G. Matvienko, and V. K. Oshlakov, Atmospheric Ocean. Opt. **35**, 19 (2022).
23. W. Liu and S. L. Chin, Opt. Express **13**, 5750 (2005).
24. X.-L. Liu, X. Lu, X. Liu, *et al.*, Opt. Express **18**, 26007 (2010).
25. B. Redding and Y.-L. Pan, Opt. Lett. **40**, 2798 (2015).
26. H. Xu, A. Azarm, J. Bernhardt, *et al.*, Chem. Phys. **360**, 171 (2009).
27. J. E. Carranza and D. W. Hahn, Anal. Chem. **74**, 5450 (2002).
28. F. Théberge, W. Liu, P. T. Simard, *et al.*, Phys. Rev. E **74**, 036406 (2006).
29. K. S. Latty, M. Burger, J. Borrero, *et al.*, Opt. Express **31**, 24652 (2023).
30. A. Becker, A. Bandrauk, and S. Chin, Chem. Phys. Lett. **343**, 345 (2001).
31. A. Becker, N. Aközbek, K. Vijayalakshmi, *et al.*, Appl. Phys. B **73**, 287 (2001).
32. I. Ghebregziabher, K. C. Hartig, and I. Jovanovic, Opt. Express **24**, 5263 (2016).

FULL REFERENCES

1. Y. Zhang, T. Zhang, and H. Li, "Application of laser-induced breakdown spectroscopy (LIBS) in environmental monitoring," Spectrochimica Acta Part B: At. Spectrosc. **181**, 106218 (2021).
2. H. Ji, Y. Ding, L. Zhang, *et al.*, "Review of aerosol analysis by laser-induced breakdown spectroscopy," Appl. Spectrosc. Rev. **56**, 193–220 (2021).
3. D. W. Hahn and M. M. Lunden, "Detection and Analysis of Aerosol Particles by Laser-Induced Breakdown Spectroscopy," Aerosol Sci. Technol. **33**, 30–48 (2000).
4. E. H. Kwapis, J. Borrero, K. S. Latty, *et al.*, "Laser Ablation Plasmas and Spectroscopy for Nuclear Applications," Appl. Spectrosc. **78**, 9–55 (2024).
5. M. Z. Martin, M.-D. Cheng, and R. C. Martin, "Aerosol Measurement by Laser-Induced Plasma Technique: A Review," Aerosol Sci. Technol. **31**, 409–421 (1999).
6. P. Diwakar, P. Jackson, and D. Hahn, "The effect of multi-component aerosol particles on quantitative laser-induced breakdown spectroscopy: Consideration of localized matrix effects," Spectrochimica Acta Part B: At. Spectrosc. **62**, 1466–1474 (2007).
7. K. S. Latty and K. C. Hartig, "Spatiotemporal Plasma-Particle Characterization of Dry Aerosols Using Nanosecond, Femtosecond, and Filament Laser-Produced Plasmas," Appl. Spectrosc. p. 000370282211494 (2022).
8. V. Hohreiter and D. W. Hahn, "Plasma-Particle Interactions in a Laser-Induced Plasma: Implications for Laser-Induced Breakdown Spectroscopy," Anal. Chem. **78**, 1509–1514 (2006).
9. P. Purohit, F. J. Fortes, and J. J. Laserna, "Atomization efficiency and photon yield in laser-induced breakdown spectroscopy analysis of single nanoparticles in an optical trap," Spectrochimica Acta Part B: At. Spectrosc. **130**, 75–81 (2017).
10. P. Dalyander, I. Gornushkin, and D. Hahn, "Numerical simulation of laser-induced breakdown spectroscopy: Modeling of aerosol analysis with finite diffusion and vaporization effects," Spectrochimica Acta Part B: At. Spectrosc. **63**, 293–304 (2008).
11. Z. Gong, Y.-L. Pan, G. Videen, and C. Wang, "Optical trapping and manipulation of single particles in air: Principles, technical details, and applications," J. Quant. Spectrosc. Radiat. Transf. **214**, 94–119 (2018).
12. T. Liu, X. Cheng, Q. Zhang, *et al.*, "Improvement of the reproducibility in LIBS single levitated aerosol particle analysis based on particle size-selectivity of photophoretic optical trap," Talanta **268**, 125326 (2024).
13. F. J. Fortes, P. Purohit, and J. J. Laserna, "Energy transfer mechanisms in laser-induced plasmas: Variation of physical traits mediated by the presence of single optically-trapped nanoparticulate material," Spectrochimica Acta Part B: At. Spectrosc. **180**, 106193 (2021).
14. C. Niu, Z. Hu, X. Cheng, *et al.*, "Individual Micron-Sized Aerosol Qualitative Analysis-Combined Raman Spectroscopy and Laser-Induced Breakdown Spectroscopy by Optical Trapping in Air," Anal. Chem. **95**, 2874–2883 (2023).
15. S. T. Järvinen, S. Saari, J. Keskinen, and J. Toivonen, "Detection of Ni, Pb and Zn in water using electrodynamic single-particle levitation and laser-induced breakdown spectroscopy," Spectrochimica Acta Part B: At. Spectrosc. **99**, 9–14 (2014).
16. P. Purohit, F. J. Fortes, and J. Laserna, "Diffusion dynamics and characterization of attogram masses in optically trapped single nanoparticles using laser-induced plasma imaging," Nano Res. **16**, 7470–7480 (2023).
17. E. Gamaly and A. Rode, "Physics of ultra-short laser interaction with matter: From phonon excitation to ultimate transformations," Prog. Quantum Electron. **37**, 215–323 (2013).
18. C. Burgos-Palop, P. Purohit, F. J. Fortes, and J. Laserna, "Ultrafast Laser Excitation Improves LIBS Performance for the Analysis of Optically Trapped Single Nanoparticles Owing to Characteristic Interaction Mechanisms," Anal. Chem. **95**, 14541–14550 (2023).
19. S. L. Chin and H. Xu, "Tunnel ionization, population trapping, filamentation and applications," J. Phys. B: At. Mol. Opt. Phys. **49**, 222003 (2016).
20. V. Tamulienė, G. Juškevičiūtė, D. Buožius, *et al.*, "Influence of tunnel ionization to third-harmonic generation of infrared femtosecond laser pulses in air," Sci. Reports **10**, 17437 (2020).
21. Z. Zhang, N. Zhang, Y. Wang, *et al.*, "Detection of 1.4 ug/m ^{3} Na^+ in aerosol at a 30 m distance using 1 kHz femtosecond laser filamentation in air," Opt. Express **31**, 6464 (2023).
22. P. A. Babushkin, G. G. Matvienko, and V. K. Oshlakov, "Determination of the Elemental Composition of Aerosol by Femtosecond Laser-Induced Breakdown Spectroscopy," Atmospheric Ocean. Opt. **35**, 19–26 (2022).
23. W. Liu and S. L. Chin, "Direct measurement of the critical power of femtosecond Ti:sapphire laser pulse in air," Opt. Express **13**, 5750 (2005).
24. X.-L. Liu, X. Lu, X. Liu, *et al.*, "Tightly focused femtosecond laser pulse in air: from filamentation to breakdown," Opt. Express **18**, 26007 (2010).
25. B. Redding and Y.-L. Pan, "Optical trap for both transparent and absorbing particles in air using a single shaped laser beam," Opt. Lett. **40**, 2798 (2015).
26. H. Xu, A. Azarm, J. Bernhardt, *et al.*, "The mechanism of nitrogen fluorescence inside a femtosecond laser filament in air," Chem. Phys. **360**, 171–175 (2009).
27. J. E. Carranza and D. W. Hahn, "Assessment of the upper particle size limit for quantitative analysis of aerosols using laser-induced breakdown spectroscopy," Anal. Chem. **74**, 5450–5454 (2002).
28. F. Théberge, W. Liu, P. T. Simard, *et al.*, "Plasma density inside a femtosecond laser filament in air: Strong dependence on external focusing," Phys. Rev. E **74**, 036406 (2006).
29. K. S. Latty, M. Burger, J. Borrero, *et al.*, "Emission characteristics of bulk aerosols excited by externally focused femtosecond filaments," Opt. Express **31**, 24652 (2023).
30. A. Becker, A. Bandrauk, and S. Chin, "S-matrix analysis of non-resonant multiphoton ionisation of inner-valence electrons of the nitrogen molecule," Chem. Phys. Lett. **343**, 345–350 (2001).
31. A. Becker, N. Aközbek, K. Vijayalakshmi, *et al.*, "Intensity clamping and re-focusing of intense femtosecond laser pulses in nitrogen molecular gas," Appl. Phys. B **73**, 287–290 (2001).
32. I. Ghebregziabher, K. C. Hartig, and I. Jovanovic, "Propagation distance-resolved characteristics of filament-induced copper plasma," Opt. Express **24**, 5263 (2016).